

An Orchestration Framework for Open System Models of Reconfigurable Intelligent Surfaces

Victor Croisfelt, *Graduate Student Member, IEEE*,

Francesco Devoti, *Member, IEEE*, Fabio Saggese, *Member, IEEE*,

Vincenzo Sciancalepore, *Senior Member, IEEE*, Xavier Costa-Pérez, *Senior*

Member, IEEE, and Petar Popovski, *Fellow, IEEE*

Abstract

To obviate the control of reflective intelligent surfaces (RISs) and the related control overhead, recent works envisioned autonomous and self-configuring RISs that do not need explicit use of control channels. Instead, these devices, named hybrid RISs (HRISs), are equipped with receiving radio-frequency (RF) chains and can perform sensing operations to act independently and in parallel to the other network entities. A natural problem then emerges: as the HRIS operates concurrently with the communication protocols, how should its operation modes be scheduled in time such that it helps the network while minimizing any undesirable effects? In this paper, we propose an orchestration framework that answers this question revealing an engineering trade-off, called the *self-configuring trade-off*, that characterizes the applicability of self-configuring HRISs under the consideration of massive multiple-input multiple-output (mMIMO) networks. We evaluate our proposed framework considering two different HRIS hardware architectures, the power- and signal-based HRISs that differ in their hardware complexity. The numerical results show that the self-configuring HRIS can offer significant performance gains when adopting our framework.

Index Terms

Reconfigurable intelligent surface, orchestration, massive MIMO.

V. Croisfelt, F. Saggese, and P. Popovski are with Aalborg Universitet, 9220 Aalborg, Denmark. F. Devoti and V. Sciancalepore are with NEC Laboratories Europe, 69115 Heidelberg, Germany. X. Costa-Pérez is with i2cat, ICREA, and NEC Laboratories Europe, 08034 Barcelona, Spain. V. Croisfelt, F. Saggese, and P. Popovski were supported by the Villum Investigator grant "WATER" from the Velux Foundation, Denmark, and part by the EU H2020 RISE-6G project under grant agreement no. 101017011.

I. INTRODUCTION

RIS is an emerging technology with a significant role on the research agenda towards 6G [1], [2]. Typically, RIS refers to a grid of elements, sometimes called meta-atoms, that enables manipulation of the electromagnetic waves beyond the classical Snell's law, allowing, for example, arbitrary changes in the reflection angle of an impinging wave by changing the reflection configuration of the phase-shifts of each element of the RIS [3]. Recently, this technology has enabled a new vision where a plethora of nearly-passive and low-complex RIS network elements can be deployed within the wireless network ecosystem, providing at least partial control over the propagation environment [4]. The envisioned benefits of RIS-aided wireless networks cover communication performance boost, electromagnetic-field exposure minimization, advanced privacy guarantees, blind technological assistance, and, many others [1], [2]. However, a major obstacle to the practical viability of RIS is the need for its real-time control and the corresponding additional control overhead required by each newly-installed RIS [5].

Many publications often consider that the control of the RIS is carried out by the base station (BS), since the latter has access to channel state information (CSI) and other relevant information, such as the actual network performance [1], [2]. On the other hand, to counteract the mentioned drawback, an alternative is to adopt self-configuring RIS designs, as depicted in Fig. 1. In those, the network operates as an open system because the RIS has to discover by itself how to collaborate with the network without or with a very limited exchange of control information. Although this idea was originally introduced over 10 years ago [6], there are still many challenges on how to deal with the increased complexity of having many elements at the RIS without impacting significantly the hardware cost and the operating expenses of the network, as recently discussed in [7]. In particular, a self-configuring RIS needs to perform a sensing process to detect the communication entities, BS and user equipments (UEs) and acquires their CSI locally to autonomously collaborate with the ongoing communication. In turn, this requires that the RIS board contains additional hardware components that enable signal reception/sensing and, thus, turn the nearly-passive RIS into a hybrid device, namely a hybrid reconfigurable intelligent surface (HRIS) [8].¹ Admittedly, this type of RIS is structurally between a classical passive RIS and a relay, since it does include the capability for radio reception, but not radio transmission [9]. However, such a sensing process may exert a negative impact on the network operation, since the

¹We refer to self-configuring RIS and self-configuring HRIS interchangeably for the rest of the paper.



Fig. 1: Internet-of-Surfaces scenario with multiple self-configuring RISs to enhance communication performance without an explicit control channel.

HRIS is self-configured concurrently with the operation of the communication protocol between the BS and the UEs. Therefore, a detailed feasibility study and orchestration framework are required to effectively have self-configuring HRISs in place, while still ensuring conventional network operations. These are even more crucial when considering massive MIMO (mMIMO) networks that became one of the most important technologies of 5G and are currently being deployed worldwide [10].

A. Related Works

RIS-assisted mMIMO networks have been considerably studied in recent years. The pioneer work [11] revealed that favorable propagation no longer holds for RIS-assisted mMIMO networks. As a result, it was shown that the maximum-ratio (MR) combining performs poorly since it leads to strong inter-user interference, and, therefore, a zero-forcing (ZF) combining strategy is then preferable. In [12]–[14], the authors analyzed the performance of RIS-assisted mMIMO networks under the consideration of imperfect CSI, different precoding and combining techniques, and different ways to optimize the reflection configuration at the RIS by using either instantaneous or statistical CSI acquired at the BS. In general, they showed that network performance increases compared to the case where the RIS is absent. In [15], the authors used the RIS to purposely break the channel reciprocity and, consequently, they were able to reduce the effect of pilot contamination often present in mMIMO networks. Furthermore, [16] proposes a solution to improve the performance of such a network for the case of mobile UEs in the presence of outdated CSI. However, in all of these works, it is assumed that the BS controls the

RIS, providing it with the necessary information to be optimized and perfectly synchronizing its functionalities according to the different operations carried out by the network.

CSI availability at the RIS is of paramount importance to properly exploit its functionality and its acquisition is one of the main challenges to be overcome [1], [2]. In [17]–[20], methods to acquire the CSI at the BS are proposed for RIS-assisted networks. However, for these methods to be feasible the BS needs to control the functioning of the RIS. HRIS hardware architecture alleviates the problem of CSI acquisition, opening novel ways to estimate the CSI locally at the HRIS itself [21]–[23]. In [24], a compressive sensing approach is proposed to reconstruct the full CSI from a subset of active elements. In [25], the received pilot signals are processed to estimate the corresponding channel. However, those methods do not exploit the network operations that are taking place in parallel to the operation of the HRIS.

The closest works to ours are [7], [26], where a self-configuring HRIS has been optimized to assist the ongoing communication and a framework has been proposed in order to do so. However, these works only consider the communication phase of the network, which is when the payload data is exchanged. Thus, the HRIS impact on the entire network operation is neglected.

B. Contributions

In this work, we propose, to the best of the authors' knowledge, the first orchestration framework that conciliates the HRIS operation modes and the operation phases of a canonical mMIMO network [27]. The self-configuring HRIS switches between two operation modes so that it can locally detect the UEs and estimate their CSI to help the communication between BS and UEs. These operation modes are the HRIS probe and reflection modes [7]. Meanwhile, the network performs the channel estimation (CHEST) and communication (COMM) phases [27]. Thus, the main question that we want to answer is: *How should the HRIS perform its operations while ascertaining minimal disruption of the network operation?* Our orchestration framework answers this question and shows an interesting engineering trade-off, called the self-configuring trade-off, which represents the price to be paid for having an open system, that is, there is no explicit control of the HRIS. Our numerical results show that the HRIS can essentially double the network performance when using our orchestration framework, where different HRIS hardware architectures were considered.

Paper Outline: The remainder of the paper is organized as follows. Sect. II presents an overview of the proposed framework and sets the basic nomenclatures and notations. In Sect. III,

we define a channel model used in the paper. In Sect. IV, we firstly introduce two HRIS architectures: the power-based and the signal-based. Then, we design the operation modes of the HRIS considering the particularities of both architectures. In Sect. V, we analytically analyze the impact of the HRIS operations on the mMIMO network performance using our proposed orchestration framework. In Sect. VI, we numerically evaluate the performance of the proposed framework. Conclusions are drawn in Sect. VII.

Notations: Vectors and matrices are denoted by bold lowercase and uppercase letters, respectively. The ij -th element of a matrix \mathbf{X} is $[\mathbf{X}]_{i,j}$, while the i -th element of a vector \mathbf{y} is y_i . Conjugate transpose, matrix transpose, and matrix Hermitian transpose operators are denoted as $(\cdot)^*$, $(\cdot)^T$, $(\cdot)^H$, respectively. The diagonal operator is $\text{diag}(\cdot)$, whereas $\|\cdot\|_2$ denotes the ℓ_2 -norm. We denote the inner product between two vectors \mathbf{x} and \mathbf{y} as $\langle \mathbf{x}, \mathbf{y} \rangle$, while \circ stands for the Hadamard product. Integer sets are represented by calligraphic letters, *e.g.*, \mathcal{A} with cardinality $|\mathcal{A}| = A$, whereas \mathbb{N} , \mathbb{R} and \mathbb{C} denote the sets of natural, real, and complex numbers respectively. The operators $\Re(\cdot)$ and $\Im(\cdot)$ return the real and the imaginary part of a number. The conditional probability distribution function (PDF) is denoted as $p(x; E)$ for the random variable x given the event E . The exponential distribution with parameter ζ is $\text{Exp}(\zeta)$, and $Q_{\chi_n^2}(x)$ denotes the right-tail distribution of a central χ_n^2 -distributed random variable x with n degrees of freedom. For a non-central one, we use the notation $Q_{\chi_n^2(\mu)}(x)$, where μ is the non-centrality parameter. Complex Gaussian distribution with mean μ and variance σ^2 is denoted as $\mathcal{CN}(\mu, \sigma^2)$.

II. PROPOSED ORCHESTRATION FRAMEWORK

In this section, we give an overview of the proposed orchestration framework. Consider a single-cell network, in which an mMIMO BS serves multiple UEs that are already scheduled.² The network operates according to a time-division duplex (TDD) protocol, whose overall frame duration is set accordingly to the coherence time of the channel [27], which defines the length of a coherence block given the respective system bandwidth. A coherence block represents the number of samples in which the channel responses can be approximated as constant and flat fading [27]. A network operator is interested in deploying a HRIS to enhance the propagation conditions. Based on the Plug&Play HRIS approach envisioned in [7], the HRIS is a transparent

²The user scheduling problem with the presence of a HRIS is related to the RIS-assisted initial access problem addressed in [28], [29], and it is out of the scope of this paper.

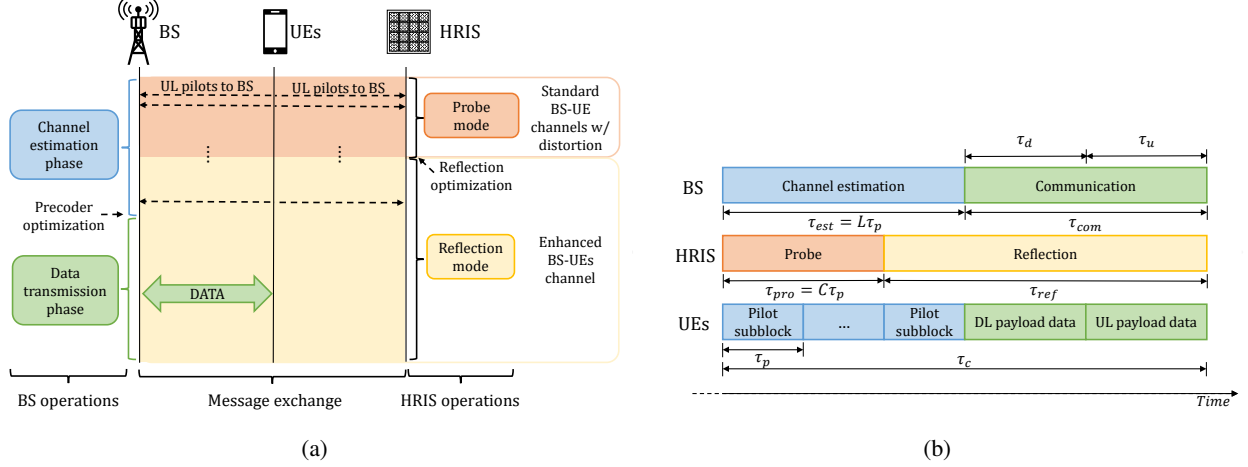


Fig. 2: Temporal evolution of the proposed orchestration framework.

device acting silently in favor of the BS and the UEs. To do so, the HRIS needs firstly to detect the BS and to acquire frame-level synchronization. This could be done based on invite packets broadcasted by the BS for UE connection establishment. In this regard, we assume that the HRIS and UEs are perfectly synchronized to the TDD protocol. In a given coherence block, the network operates according to the following *operation phases* [27]:

- *CHEST phase*: The UEs transmit pilot signals so that the BS can acquire the CSI to make efficient use of the massive number of antennas. Based on channel reciprocity implied by the TDD operation, the obtained CSI at the BS side holds for both uplink (UL) and downlink (DL) directions.
- *COMM phase*: This phase comprises the UL and DL data traffic, while the BS exploits the CSI obtained during the CHEST to spatially separate the UEs based on transmit precoding and receive combining techniques.

While the operation phases run, the HRIS self-configures *concurrently* and *autonomously* assists the network as an open system since there is no control information exchange between the BS and the HRIS. To do so, we consider that the HRIS alternates between two *operation modes* in a given coherence block [7]:

- *Probe mode*: The purpose of this mode is for the HRIS to probe the environment for UEs being served by BS. After detecting the UEs, the HRIS estimates the CSI of the HRIS-UE channels. In principle, the HRIS also wishes to acquire the CSI of the BS-HRIS channels. However, based on the assumption that the BS and the HRIS are static, the coherence time

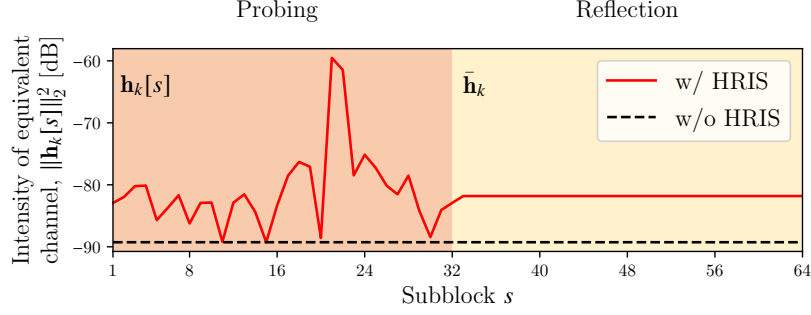


Fig. 3: Example of the temporal evolution of the equivalent BS-UE channel during the mMIMO channel estimation phase considering a scenario with (w/) and without (w/o) an HRIS deployed. The HRIS executes a power-based probing phase with $L = 64$.

of the BS-HRIS channel is longer than the HRIS-UE channels [30]. As a consequence, we will consider that the HRIS has a perfect knowledge of the BS-HRIS channels, acquired previously, *e.g.*, by listening to the pilot signals sent periodically by the BS. Note that the HRIS can also exploit the channel reciprocity resulting from the TDD operation and, consequently, the HRIS can just get the CSI in the UL direction and extrapolate it to the DL direction.³

- *Reflection mode:* The HRIS optimizes the reflection configuration of its elements to enhance the channel conditions of the UEs and, consequently, maximizing a given communication key performance indicator (KPI) of the network. Such optimization is based on the set of detected UEs and their CSI obtained during the probe mode.

Since the HRIS needs to activate both operation modes within a coherence block, it can affect the network operation phases in an undesirable way, as we will discuss shortly. Therefore, we need to conveniently *orchestrate* the HRIS operation modes to suit the network operation phases and maximize the benefit of self-configured HRIS deployments, mitigating possible negative impacts of one over the other.

Orchestration Framework: Fig. 2a summarizes the operations of the BS, HRIS, and UEs and their temporal evolution occurring within a coherence block according to the proposed orchestration framework. To effectively benefit from the HRIS deployment, we arrange its

³We will assume that channel reciprocity is perfectly achieved by means of carefully designed hardware or the use of specific algorithms [27] to allow us to focus on discussing the main ideas behind our proposed framework. Future research can explore what happens if channel reciprocity is violated.

operations according to the operation phases of the mMIMO system by proposing two design rules. First, the HRIS probe mode is partially overlapped with the CHEST phase. The reason behind this choice is that the HRIS can take advantage of the pilot signals to detect the UEs and subsequently estimate their CSI. Second, the HRIS must be in reflection mode before the end of the CHEST phase and during the entire COMM phase. This is because, as depicted in Fig. 3, the BS-UE equivalent channel is not stable during the probe mode since the HRIS can affect the propagation environment to sense the UEs. This can affect the quality of the CSI obtained at the BS. Hence, imposing the start of the reflection mode to occur during the CHEST phase, we allow the BS to collect a certain number of samples of the stable, enhanced equivalent BS-UE channels that are going to be present during the communication phase. The distortion introduced by the HRIS is formally defined as follows.

Definition 1 (Probe distortion). *The probe distortion is the distortion introduced into the CSI acquisition at the BS side as a consequence of the HRIS probe mode altering the surrounding propagation environment, as shown in Fig. 3.*

Due to the probe distortion and the consequent CSI mismatch, the BS might spatially separate the UEs incorrectly, potentially hindering network performance. Ideally, to avoid the aforementioned problem, the CHEST phase should take place only when the HRIS is in reflection mode in such a way the BS only gets the CSI of the stable channel that is supporting the data transfer. However, the BS is unaware of the HRIS operation due to the openness of the system, that is, there is no feedback between the BS and HRIS. Hence, the BS cannot start the CHEST after the HRIS probe completion. Therefore, the HRIS should minimize its probe duration and switch to the reflection mode as soon as possible while the CHEST phase of the network is ongoing. This generates a very interesting engineering trade-off: reducing the probe time worsens the HRIS probe mode performance, which can reduce the effectiveness of the reflection mode since less UEs can be detected; at the same time, it improves the accuracy of the CSI at the BS due to the higher number of samples of the stable channel state. Vice versa, increasing the probe duration increases the probe distortion, reducing CSI accuracy at the BS side, while improving the probe mode performance and obtaining a better reflection configuration. We define it below.

Definition 2 (Self-configuring trade-off). *The self-configuring trade-off consists in balancing the performance of the HRIS probe mode and of the CHEST phase by setting the probe duration.*

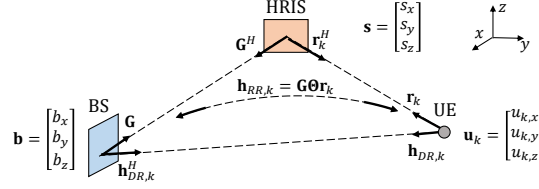


Fig. 4: Geometrical representation of the considered scenario including the BS, the RIS, and the UE.

This trade-off can be seen as the price to be paid for the autonomous operation of the HRIS and requires a careful analysis to understand its impact on the overall network performance.

A. System Model

Formally, we assume that the BS is equipped with an M -sized uniform linear array (ULA) and is simultaneously serving K single-antenna UEs assisted by an HRIS. We further denote as K_{\max} the maximum number of UEs that can be supported by the network at a coherence block. Moreover, the HRIS is comprised of $N = N_x N_z$ elements arranged as a uniform planar array (UPA), where N_x and N_z denote the number of elements along the x - and z -axis, respectively. To simplify notation, we introduce the index sets \mathcal{M} , \mathcal{K} , and \mathcal{N} to index BS antennas, UEs, and HRIS elements, respectively. Based on the TDD operation mode [27], the time-frequency resources are divided into coherence blocks of τ_c *channel uses or samples* indexed by \mathcal{T}_c . The size of a coherence block is mainly determined by the propagation environment, the carrier frequency f_c with corresponding wavelength λ_c , and by the UE mobility since the more dynamic channels are among the BS-UEs and the HRIS-UEs. Thus, we assume that τ_c is selected such that the BS-UEs channel responses are constant and frequency flat within a coherence block. Due to the same propagation environment, we consider that this latter assumption also applies to the HRIS-UE channels.

In order to reflect incoming waves towards a desired direction, the HRIS is capable of configuring the phase shift of each of its elements. A particular combination of phase shifts is called *HRIS configuration* and is denoted as a diagonal matrix $\mathbf{\Theta} \in \mathbb{C}^{N \times N}$, where only diagonal elements are non-zero. Focusing on the UL and a particular UE k for $k \in \mathcal{K}$, the equivalent BS-UE channel $\mathbf{h}_k \in \mathbb{C}^M$ is

$$\mathbf{h}_k(\mathbf{\Theta}) = \mathbf{h}_{DR,k} + \mathbf{h}_{RR,k}(\mathbf{\Theta}), \quad (1)$$

where $\mathbf{h}_{\text{DR},k} \in \mathbb{C}^M$ is the **direct** channel and $\mathbf{h}_{\text{RR},k} \in \mathbb{C}^M$ is the **resulting reflected** channel, as depicted in Fig. 4. Note that the resulting reflected channel is a function of the HRIS configuration and so it is the equivalent channel. Moreover, observe that the channel over the reflected path $\mathbf{h}_{\text{RR},k}$ can be written in terms of the HRIS-UE channel $\mathbf{r}_k \in \mathbb{C}^N$ and the BS-HRIS channel $\mathbf{G} \in \mathbb{C}^{M \times N}$. For now, we do not specify the propagation model as the framework can be applied irrespective of it. For our proposed framework to be meaningful, we make the following assumption about how the HRIS operates.

Assumption 1 (HRIS configuration change). *Consider a subblock as a group of samples within the same coherence block. We assume that the HRIS is able to change its configuration Θ on a subblock basis. We denote as $\Theta[s]$ the configuration impressed at the self-configuring HRIS at the s -th subblock where s is taken from indexing a partition of \mathcal{T}_c . In the special case that a subblock is comprised of a single sample, we have that $s \in \mathcal{T}_c$.*

The above assumption is in line with the current development of the RIS technology. Indeed, an RIS requires a time ranging from microseconds to milliseconds to change its configuration [31], which might correspond to the duration of a subblock of an orthogonal frequency division multiplexing (OFDM) frame. As a consequence, the equivalent channel also changes on a subblock basis owing to the possibility of changing the configuration at HRIS. Thus, (1) can be rewritten as:

$$\mathbf{h}_k[s] = \mathbf{h}_{\text{DR},k} + \mathbf{h}_{\text{RR},k}[s], \quad (2)$$

where $\mathbf{h}_{\text{DR},k}$ is not affected by the HRIS configuration change.

B. Detailed network operation

Figure 2b illustrates how the coherence block is sliced simultaneously into the different network operation phases and HRIS operation modes. Specifically, we let τ_{chest} and τ_{comm} be the number of samples comprising the network CHEST and COMM phases, respectively, such that $\tau_c = \tau_{\text{chest}} + \tau_{\text{comm}}$. The COMM phase can be further divided into τ_d and τ_u samples for DL and UL payload data traffic, respectively; that is, $\tau_{\text{comm}} = \tau_d + \tau_u$. Simultaneously, we let $\tau_{\text{prob}} \leq \tau_{\text{chest}}$ and τ_{refl} be the number of samples in which the HRIS operates in probe and reflection modes, respectively, with $\tau_c = \tau_{\text{prob}} + \tau_{\text{refl}}$. Based on the self-configuring trade-off, the probing duration should be designed to have $\tau_{\text{prob}} \ll \tau_{\text{chest}}$. However, τ_{prob} should be sufficient to accurately detect

UEs so as to obtain an effective HRIS configuration during the reflection mode that actually helps to improve the network performance.

During connection establishment, the BS performs a pilot assignment $p(i) : \mathcal{K} \mapsto \mathcal{T}_p$, where each UE is assigned to a pilot signal in a deterministic way. In other words, $p(i) \in \mathcal{T}_p$ represents the index of the pilot signal assigned to a UE $i \in \mathcal{K}$. Each pilot $\Phi_t \in \mathbb{R}^{\tau_p}$ spans for τ_p samples. The pilots are selected from a pilot codebook $\Phi \in \mathbb{R}^{\tau_p \times \tau_p}$ with columns representing the τ_p pilots enumerated by the index set $\mathcal{T}_p = \{1, \dots, \tau_p\} \subset \mathcal{T}_c$. We assume the following about the pilot codebook.

Assumption 2 (Orthogonal pilot codebook). *The pilot codebook contains orthogonal sequences, such that $\Phi_t^H \Phi_{t'} = \tau_p$ if $t = t'$ and $\Phi_t^H \Phi_{t'} = 0$ for $t \neq t'$, $\forall t, t' \in \mathcal{T}_p$. In particular, we assume $\Phi = \sqrt{\tau_p} \mathbf{I}_{\tau_p}$. To avoid pilot contamination [27], the maximum number of UEs supported by the network is equal to the pilot length, i.e., $K_{\max} = \tau_p$. We further assume that HRIS knows Φ , and hence K_{\max} , by communicating with the BS right after establishing its connection without imposing a serious overhead, as the HRIS only needs to ask once.*

Assumption 2 is based on the rule-of-thumb for the selection of the number of pilots described in [27]. As a consequence of the above design and the rules of our orchestration framework introduced previously, an issue emerges if we take the duration of the CHEST phase to be equal to the pilot length $\tau_{\text{chest}} = \tau_p$. To see it, consider the following example.

Example 1. *Consider that $K = K_{\max} = \tau_p = 2$ and that $\tau_{\text{chest}} = \tau_p$. Assume that UE 1 is assigned to the pilot $[\sqrt{2}, 0]^T$ and UE 2 has $[0, \sqrt{2}]^T$. As we want that $\tau_{\text{prob}} \ll \tau_{\text{chest}}$ while it being greater than 0, we choose $\tau_{\text{prob}} = 1$. In this case, the HRIS would just receive the first entries of the pilots sent by the UEs. Since the first entry of UE 2 is 0, the HRIS would be able to detect only UE 1 no matter what UE 2 did.*

To solve the above problem, we propose the following pilot repetition strategy.⁴

Assumption 3 (CHEST duration – pilot repetition). *We assume that each UE re-transmits its pilot for $L > 1$ times such that $\tau_{\text{chest}} = L\tau_p$. We refer to each of the repetitions as a pilot*

⁴Another way around this problem would be to properly design the pilot codebook. However, to keep us focused on showing the functionality of our proposed framework and the basic insights of the self-configuring trade-off, we choose to assume the orthogonal pilot sequences design. Future work may relax this assumption and disregard the pilot's repetition strategy.

subblock, indexed by the set \mathcal{L} , where \mathcal{L} indicates a partition of the set \mathcal{T}_p . We index variables that occur on a pilot-subblock basis by introducing a $[l]$ in front of it.

This assumption allows us to effectively accommodate the HRIS probe within the CHEST phase while also being able to control the size of the former avoiding the problem seen in Example 1. Based on the above assumption and the self-configuring trade-off, we assume the following about the duration of the HRIS probe.

Assumption 4 (Probe duration). *We assume the duration of the HRIS probe to be an integer multiple of the pilot length τ_p satisfying $\tau_{\text{prob}} \ll \tau_{\text{chest}}$. Hence, the HRIS probe spans for $\tau_{\text{prob}} = C\tau_p \ll \tau_{\text{chest}} = L\tau_p \implies C \ll L$ with $C > 1$ being the number of pilot subblocks in which the HRIS probes and $C \subseteq \mathcal{L}$. We index variables that occur on a subblock basis, but during probing, by introducing a $[c]$ in front of it.*

As a result, the time in which the HRIS operates in reflection mode is $\tau_{\text{refl}} = \tau_c - \tau_{\text{prob}} = \tau_c - C\tau_p$. Thus, we have the following remark about the self-configuring trade-off.

Remark 1 (Self-configuring trade-off). *The self-configuring trade-off of the proposed orchestration framework relies on choosing $\tau_{\text{prob}} = C\tau_p$ or, equivalently, C such that the network performance assisted by the HRIS is higher than the one in which the network works alone.*

Our goal is to further characterize the above trade-off by properly designing the HRIS operation modes and measuring how the network performance is affected by them.

III. CHANNEL MODEL

In this section, we present a conventional channel model for the scenario of interest to be able to design the algorithmic aspects of the operation modes of the self-configuring HRIS. For clarity of presentation, we ignore the subblock indexing used in (1) and derive the channel model by assuming just a single sample.

A. Array steering vectors and pathloss

Denote as $\mathbf{b} \in \mathbb{R}^3$, $\mathbf{e} \in \mathbb{R}^3$, and $\mathbf{u}_k \in \mathbb{R}^3$ the locations of the BS center, of the HRIS center, and of the k -th UE for $k \in \mathcal{K}$, respectively. The position of the m -th BS element is $\mathbf{b}_m \in \mathbb{R}^3$ for $m \in \mathcal{M}$, while of the n -th HRIS element is $\mathbf{e}_n \in \mathbb{R}^3$ for $n \in \mathcal{N}$. To avoid mutual coupling, the

inter-element distances in both BS and the HRIS arrays are set to $\lambda_c/2$. Let $\mathbf{a}_B(\mathbf{p}) \in \mathbb{C}^M$ and $\mathbf{a}_H(\mathbf{p}) \in \mathbb{C}^N$ denote the BS and HRIS array response vectors towards a generic location $\mathbf{p} \in \mathbb{R}^3$, respectively. By considering the HRIS, the n -th element of the array response vector $\mathbf{a}_H(\mathbf{p})$ is [7]

$$[\mathbf{a}_H(\mathbf{p})]_n \triangleq e^{j\langle \mathbf{k}(\mathbf{p}, \mathbf{e}), (\mathbf{e}_n - \mathbf{e}) \rangle}, \text{ with } \mathbf{k}(\mathbf{p}, \mathbf{e}) \triangleq \frac{2\pi}{\lambda} \frac{\mathbf{p} - \mathbf{e}}{\|\mathbf{e} - \mathbf{p}\|_2}, \quad (3)$$

being $\mathbf{k}(\mathbf{p}, \mathbf{e}) \in \mathbb{R}^3$ the wave vector. The array steering vector from the BS is derived in a similar way. Next, the pathloss model between two generic locations $\mathbf{p}, \mathbf{q} \in \mathbb{R}^3$ is defined as [7]

$$\gamma(\mathbf{p}, \mathbf{q}) \triangleq \gamma_0 \left(\frac{d_0}{\|\mathbf{p} - \mathbf{q}\|_2} \right)^\beta, \quad (4)$$

where γ_0 is the channel power gain at a reference distance d_0 and β is the pathloss exponent. In principle, we assume that the direct paths between BS and UEs are under pathloss exponent β_B , while BS-HRIS and HRIS-UE channels suffer from pathloss exponent β_H .

B. Rician fading

Focusing on the UL direction and in a particular UE k for $k \in \mathcal{K}$, we assume an i.i.d. Rician fading model for each of the links between the BS-UEs and HRIS-UEs, while the links between BS-HRIS are assumed to be line-of-sight (LoS) dominant. This latter assumption is valid if the RIS is deployed to have a strong LoS towards the BS [32]. Thus, recalling eq. (1), we have

$$\mathbf{h}_{\text{DR},k} \sim \mathcal{CN}(\bar{\mathbf{h}}_{\text{DR},k}, \sigma_{\text{DR}}^2 \mathbf{I}_M) \quad \text{and} \quad \mathbf{r}_k \sim \mathcal{CN}(\bar{\mathbf{r}}_k, \sigma_{\text{RR}}^2 \mathbf{I}_N), \quad (5)$$

where $\bar{\mathbf{h}}_{\text{DR},k}$ and $\bar{\mathbf{r}}_k$ are the LoS coefficients, while σ_{DR}^2 and σ_{RR}^2 are the power of the non-line-of-sight (NLoS) components. Based on (3) and (4), the LoS coefficients are computed as

$$\bar{\mathbf{h}}_{\text{DR},k} = \sqrt{\gamma(\mathbf{b}, \mathbf{u}_k)} \mathbf{a}_B(\mathbf{u}_k), \quad \bar{\mathbf{r}}_k \triangleq \sqrt{\gamma(\mathbf{u}_k, \mathbf{e})} \mathbf{a}_H(\mathbf{u}_k), \quad \text{and} \quad \mathbf{G} \triangleq \sqrt{\gamma(\mathbf{b}, \mathbf{e})} \mathbf{a}_B(\mathbf{e}) \mathbf{a}_H^H(\mathbf{b}). \quad (6)$$

Let $\mathbf{\Theta} = \text{diag}[e^{j\theta_1}, \dots, e^{j\theta_N}]$ be a HRIS configuration with $\theta_n \in [0, 2\pi]$ denoting the phase shift impressed by the n -th HRIS element for $n \in \mathcal{N}$. Thus, the channel over the reflected path is

$$\mathbf{h}_{\text{RR},k} = \sqrt{\eta} \mathbf{G} \mathbf{\Theta} \mathbf{r}_k, \quad \text{such that} \quad \mathbf{h}_{\text{RR},k} \sim \mathcal{CN}(\sqrt{\eta} \mathbf{G} \mathbf{\Theta} \bar{\mathbf{r}}_k, N \sigma_{\text{RR}}^2 \mathbf{I}_M), \quad (7)$$

where $\eta \in [0, 1]$ represents the fraction of the received power that the HRIS reflects back to the environment. Finally, the equivalent BS-UE channel is

$$\mathbf{h}_k = \mathbf{h}_{\text{RR},k} + \mathbf{h}_{\text{DR},k}, \quad \text{such that} \quad \mathbf{h}_k \sim \mathcal{CN}(\bar{\mathbf{h}}_{\text{DR},k} + \sqrt{\eta} \mathbf{G} \mathbf{\Theta} \bar{\mathbf{r}}_k, (\sigma_{\text{DR}}^2 + N \sigma_{\text{RR}}^2) \mathbf{I}_M), \quad (8)$$

which follows from the assumption of independence between the BS-UE and HRIS-UE channels.

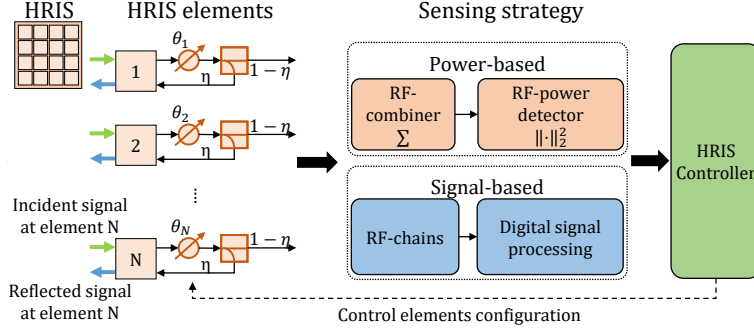


Fig. 5: Power- and signal-based hardware implementations of the self-configuring HRIS.

IV. SELF-CONFIGURING HRIS

In this part, we detail the operation of the self-configuring HRIS. First, we present two possible hardware implementations of the HRIS widely accepted in the literature. Our goal with this is to show how the algorithmic design of the HRIS operating modes depends on the available hardware architecture and later show how the network performance varies with this. We then present the basic features that constitute the probe mode. Thus, we propose two HRIS probe strategies compliant with the two different HRIS hardware architectures. For simplicity, when deriving these procedures, we chose not to overload the notation indicating signals related to each of the hardware implementations. Therefore, one should assume that the derivations in the following subsections are described independently. Finally, we present a method to calculate the reflection configurations when the HRIS operates in reflection mode, which is common to both hardware architectures.

A. HRIS Implementation

Fig. 5 depicts the two considered HRIS hardware architectures. In both, the joint reflection and absorption capabilities of the elements are realized through directional couplers. Their operation is determined by the parameter $\eta \in [0, 1]$ that represents the fraction of the received power reflected back to the environment, while $1 - \eta$ is the amount of power absorbed and used for digital signal processing (DSP) at the HRIS [21]. It is worth highlighting that both reflected and absorbed signals are subject to the phase shifts impressed by the HRIS elements. The two considered hardware architectures differ in how the absorbed signals can be processed as follows:

- 1) *Power-based HRIS*: The HRIS is equipped with a single radio frequency (RF) chain which combines the absorbed signals coming from all the elements. A power detector

then measures the received power of the superposition of the absorbed signals. The DSP capabilities are applied on this measured power [7]. In a way, this hardware architecture is the most cost and energy efficient at the price of lower performance.

- 2) *Signal-Based HRIS*: The HRIS is provided with an RF chain for each element, which is capable of outputting separated digital data streams. Thus, DSP techniques can be applied over the N acquired samples [21]. In a way, this hardware architecture is the most performance efficient at the price of higher cost and energy consumption.

The clear trade-off in the choice of hardware is between the higher cost and energy consumption and the higher computational capacity and, consequently, higher HRIS performance. Our goal is to assess how this trade-off also affects the network performance, seeking to verify the appeal of these architectures in enabling self-configuring HRIS in practice.

B. Probe Mode: General Considerations

Based on Assumptions 3 and 4, the UEs transmit pilots following the CHEST phase while the HRIS probes. The superimposed pilots $\mathbf{\Pi}[c] \in \mathbb{C}^{N \times \tau_p}$ transmitted towards the HRIS at the c -th pilot subblock are

$$\mathbf{\Pi}[c] \in \mathbb{C}^{N \times \tau_p} = \sqrt{\rho} \sum_{i \in \mathcal{K}} \mathbf{r}_i \Phi_{p(i)}^\top \quad (9)$$

where ρ is the UE transmit power, $p(i)$ denotes the pilot assigned to the i -th UE by the BS, and \mathbf{r}_i is the HRIS-UE channel of the i -th UE, as in (5). According to Assumption 2, the above expression implies that at most only the channel of a single UE can be observed per pilot. Otherwise, a pilot is considered unused if no UE was assigned to it. *At a given coherence block, the HRIS does not know which pilots are being used and which UEs are transmitting and, consequently, the HRIS is unaware of their CSI. The goal of the probe mode is to resolve those.*

According to Assumption 1, we consider that the HRIS can change its configuration to help in probing UEs. For example, the HRIS can scan the environment for UEs by changing its configurations, acting as a radar. We refer to configurations designed to help to probe as *probe configurations*. A probe configuration is assumed to change on a pilot subblock basis by following Assumption 4. From this assumption, we will limit ourselves to the case that a probe configuration codebook is available at the HRIS comprised of C configurations and is denoted as

$$\Theta_P = \{\Theta_P[c] \mid c \in C\}. \quad (10)$$

Below, we provide two alternatives to conduct the HRIS probe for the respective power- and signal-based HRIS hardware architectures. The proposed methods design the above codebook in different ways to exploit the peculiarities of each considered HRIS hardware.

C. Probe Mode: Power-Based HRIS

Similar to the approach proposed in [7] and to overcome the lack of DSP capabilities, the power-based HRIS probes for UEs by sweeping through the probe configurations in Θ_P . The HRIS thus acts in a way to scan the environment in search of UEs. For simplicity, we consider that the number of directions is the same as the number of pilot subblocks. Then, we build the probe configuration codebook to slice the area of interest into C uniform sectors over both elevation and azimuth domains with $C = C_{\text{el}}C_{\text{az}}$ being decomposed into elevation and azimuth directions, respectively. The n -th diagonal element of the c -th probe configuration is

$$[\Theta_P[c]]_{n,n} = e^{j\langle \mathbf{k}(\mathbf{p}[c], \mathbf{e}), (\mathbf{e}_n - \mathbf{e}) \rangle}, \quad (11)$$

for $n \in \mathcal{N}$ and $c \in C$ and with the c -th position being probed as

$$\mathbf{p}[c] = [\sin \psi_{\text{el}}[c] \cos \psi_{\text{az}}[c], \sin \psi_{\text{el}}[c] \sin \psi_{\text{az}}[c], \cos \psi_{\text{el}}[c]]^T, \quad (12)$$

with angular directions being

$$\psi_{\text{el}}[c] = \frac{\pi}{C_{\text{el}}} \left(\text{mod}_{C_{\text{el}}}(c-1) + \frac{1}{2} \right) \text{ and } \psi_{\text{az}}[c] = \frac{\pi}{C_{\text{az}}} \left(\frac{c-1 - \text{mod}_{C_{\text{el}}}(c-1)}{C_{\text{el}}} + \frac{1}{2} \right). \quad (13)$$

Following the above, the c -th configuration $\Theta_P[c] \in \Theta_P$ is loaded at the HRIS during the transmission of the c -th pilot subblock. Let $\theta_P[c] = [e^{j\theta_1}, \dots, e^{j\theta_N}]^T \in \mathbb{C}^N$ denote the diagonal elements of $\Theta_P[c]$. Based on (9) and after the RF-combiner in Fig. 5, the power-based HRIS receives the c -th pilot subblock signal $\mathbf{y}[c] \in \mathbb{C}^{\tau_p}$ as

$$(\mathbf{y}[c])^T = \sqrt{1-\eta}\sqrt{\rho}(\theta_P[c])^H \left(\sum_{i \in \mathcal{K}} \mathbf{r}_i \Phi_{p(i)}^T \right) + (\mathbf{n}[c])^T, \quad (14)$$

where $\mathbf{n}[c] = [n_1[c], \dots, n_{\tau_p}[c]]^T \in \mathbb{C}^{\tau_p} \sim \mathcal{CN}(0, N\sigma_H^2 \mathbf{I}_{\tau_p})$ is the receiver noise at the HRIS after the RF-combiner with σ_H^2 being the HRIS noise power.⁵ According to Assumption 2, no pilot contamination occurs between the UEs assigned to the various pilots through the assignment $p(i)$, $\forall i \in \mathcal{K}$; therefore, the entry $t = p(k)$, $k \in \mathcal{K}$, of the above sequence, can be rewritten as

$$y_{p(k)}[c] = \sqrt{1-\eta}\sqrt{\rho}\sqrt{\tau_p}(\theta_P[c])^H \mathbf{r}_k + n_{p(k)}[c]. \quad (15)$$

⁵The receiver noise is assumed to be i.i.d. over different subblocks.

The above signal is then fed to a power detector, yielding

$$\alpha_{p(k)}[c] = |y_{p(k)}[c]|^2 = |A_k[c]|^2 + 2\Re\{A_k[c]n_{p(k)}[c]\} + |n_{p(k)}[c]|^2, \quad (16)$$

where $A_k[c] = \sqrt{1 - \eta}\sqrt{\rho}\sqrt{\tau_p}(\theta_P[c])^H \mathbf{r}_k$. The power-based HRIS can store and digitally process the signals $\alpha_{p(k)}[c]$, $\forall p(k) = t \in \mathcal{T}_p$. However, eq. (16) is valid only if the t -th pilot is being used in subblock $c \in C$, which might not be the case. In the following, we describe the probing procedure for the power-based HRIS employed to detect UEs and obtain their local CSI.

Probing Procedure: Consider a given pilot subblock $c \in C$ where the c -th configuration is loaded at the HRIS according to (11). Since the HRIS knows the pilot codebook Φ (see Assumption 2), it first checks which pilots are active in the given subblock and stores the associated pilot mapping in the set $\mathcal{T}_p[c] = \{t' \in \mathcal{T}_p \mid \exists p(i) = t', \forall i \in \mathcal{K}\} \subseteq \mathcal{T}_p$. Next, the HRIS detects if there are UEs in the direction probed by the c -th configuration by applying the following binary hypothesis test over each one of the active pilots $t' \in \mathcal{T}_p[c]$ [33]:

$$\begin{aligned} \mathcal{H}_0^{(k)}[c] : \alpha_{p(k)}[c] &= |n_{p(k)}[c]|^2 \implies A_k[c] = 0, \\ \mathcal{H}_1^{(k)}[c] : \alpha_{p(k)}[c] &= |A_k[c]|^2 + 2\Re\{A_k[c]n_{p(k)}[c]\} + |n_{p(k)}[c]|^2 \implies A_k[c] \neq 0. \end{aligned} \quad (17)$$

where we remark the one-to-one mapping $p(k) = t', \forall t' \in \mathcal{T}_p[c]$. We consider that the HRIS does not have any knowledge about the distribution of the HRIS-UE channels. Therefore, the complex magnitude $A_k[c]$ is assumed to be a deterministic signal unknown to the HRIS.⁶ Moreover, we assume that the HRIS does know the noise parameter σ_H^2 by performing some estimation process over time. Thus, the generalized likelihood ratio test (GLRT) decides $\mathcal{H}_1^{(k)}[c]$ if [33, p. 200]:

$$\frac{p(\alpha_{p(k)}[c]; f_{\text{ML}}(A_k[c]), \mathcal{H}_1^{(k)}[c])}{p(\alpha_{p(k)}[c]; \mathcal{H}_0^{(k)}[c])} > \epsilon_s, \quad (18)$$

where $f_{\text{ML}}(A_k[c])$ is the maximum-likelihood estimator (ML) of *a function of the desired signal* since the form of the desired signal is assumed to be unknown by the HRIS. To obtain a more meaningful test, we need to get the distributions of the numerator and denominator of the left-hand side term of (18). From (17), we obtain for the denominator that

$$p(\alpha_{p(k)}[c]; \mathcal{H}_1^{(k)}[c]) \sim \text{Exp}\left(\frac{1}{2} \frac{1}{N\sigma_H^2}\right). \quad (19)$$

⁶In principle, the HRIS could rely on Bayesian tests to obtain a better probing performance if it knew the distribution of the HRIS-UE channels. However, assuming that the HRIS has such knowledge would go against the core idea of HRISs of being very low-energy consumption and resource-constrained devices.

To find a closed-form expression for the numerator of (18), we rewrite the signal under $\mathcal{H}_1^{(k)}$ as

$$\alpha_{p(k)}[c] = |A_k[c]|^2 + 2\Re\{A_k[c]n_{p(k)}[c]\} + |n_{p(k)}[c]|^2 \stackrel{(a)}{\approx} |A_k[c]|^2 + |n_{p(k)}[c]|^2, \quad (20)$$

where in (a) we approximate the signal by arguing that, on average, the noise contribution would be zero because of its zero mean. Hence, we get for the numerator that

$$p\left(\alpha_{p(k)}[c]; f_{\text{ML}}(A_k[c]), \mathcal{H}_1^{(k)}[c]\right) \sim \frac{1}{2N\sigma_H^2} \exp\left(-\frac{1}{2N\sigma_H^2} (\alpha - f_{\text{ML}}(A_k[c]))\right), \quad (21)$$

where $f_{\text{ML}}(A_k[c]) = \alpha_{p(k)}[c]$ for $f(A_k[c]) = |A_k[c]|^2$. By plugging (19) and (21) into (18), the HRIS decides that UE $k \in \mathcal{K}$ is detected if

$$\alpha_{p(k)}[c] \gtrsim 2N\sigma_H^2\epsilon_s' = \epsilon_s', \quad (22)$$

whose closed form expression of performance can be found $N \rightarrow \infty$ [33] as

$$P_D^{(k)}[c] = e^{-\frac{1}{2N\sigma_H^2}(\epsilon_s' - \alpha_{p(k)}[c])} \text{ and } P_{\text{FA}}^{(k)}[c] = e^{-\frac{1}{2N\sigma_H^2}\epsilon_s'}, \quad (23)$$

where $P_D^{(k)}[c]$ and $P_{\text{FA}}^{(k)}[c]$ are the probabilities of detection and false alarm for detecting UE k transmitting the $p(k)$ -th pilot within the c -th subblock, respectively. However, due to the approximation made in (20), the above performance measures provide an optimistic estimate of the real performance. More importantly, these measures also vary with the channel realizations, that is, with the fact that $A_k[c]$ is actually a random variable based on the channel model presented in Section III. Nevertheless, we consider that the above measures are useful for setting a meaningful threshold parameter ϵ_s' .

After performing the test in (17) over each active pilot $t' \in \mathcal{T}_p[c]$, the HRIS stores the detected UEs in the set $\mathcal{K}_D[c] = \{k \in \mathcal{K} | \mathcal{H}_1^{(k)}[c] \text{ is true}\} \subseteq \mathcal{K}$. The above process is repeated over all subblocks $c \in \mathcal{C}$, and the HRIS can aggregate the detection results over all the subblocks. As a result, the HRIS stores all the detected UEs and the configuration proving the higher received power as

$$\mathcal{K}_D = \bigcup_{c \in \mathcal{C}} \mathcal{K}_D[c] \quad \text{and} \quad c_k^\star = \arg \max_{c \in \mathcal{C}} \alpha_{p(k)}[c], \quad \forall k \in \mathcal{K}_D. \quad (24)$$

Since the power-based HRIS has as input only the power measures of the pilot signals, as in (16), it is not able to explicitly estimate the HRIS-UE channels \mathbf{r}_k 's of the detected UEs. Nevertheless, we are just interested in estimating the angle of arrival of the UEs, that is, $\angle \mathbf{r}_k$, since its reflection mode is essentially based on this information. Therefore, the best the HRIS can do is to use the direction given by the configuration providing the higher power in the probe configuration

codebook as a way to estimate the angle of arrival of the UEs. We define the HRIS local CSI acquired by the probing mode for user $k \in \mathcal{K}_D$ as

$$\hat{\mathbf{\Theta}}_k = \mathbf{\Theta}_P [c_k^*]. \quad (25)$$

We also compute weights ω_k to measure the importance of the k -th UE to the HRIS. This can be measured by the received power from a detected UE to the HRIS in relation the other UEs:

$$\omega_k = \frac{\sqrt{\alpha_{p(k)} [c_k^*]}}{\sum_{i \in \mathcal{K}_D} \sqrt{\alpha_{p(i)} [c_i^*]}}. \quad (26)$$

D. Probe Mode: Signal-Based HRIS

With the signal-based HRIS hardware, the HRIS has more DSP capabilities available and can process the received signals coming from all antennas simultaneously. Because of this, we start by observing that the HRIS can always reverse back the effect of the impressed probe configuration $\mathbf{\Theta}_P[c]$ digitally at the price of increased computational effort, which involves multiplying the received signal by $\mathbf{\Theta}_P[c]^{-1}$ at a given sample that comprises the c -th pilot subblock for $c \in C$. For convenience, we then assume that $\mathbf{\Theta}_P[c] = \mathbf{I}_N$, $\forall c \in C$. Based on this and (9), the signal-based HRIS receives the c -th pilot subblock signal $\mathbf{Y}_c \in \mathbb{C}^{N \times \tau_p}$ as

$$\mathbf{Y}[c] = \sqrt{1 - \eta} \sqrt{\rho} \sum_{i \in \mathcal{K}} \mathbf{r}_i \Phi_{p(i)}^T + \mathbf{N}[c], \quad (27)$$

where $\mathbf{N}[c] \in \mathbb{C}^{N \times \tau_p}$ is the receiver noise matrix with columns distributed according to $\mathbf{n}_t[c] \sim \mathcal{CN}(0, \sigma_H^2 \mathbf{I}_N)$. From Assumption 2, the HRIS knows the pilot codebook and can therefore correlate the received signal with each one of the pilots. Assuming the pilot $t \in \mathcal{T}_p$ is mapped to UE $k \in \mathcal{K}$, i.e., $p(k) = t$, its de-correlated received signal is

$$\tilde{\mathbf{y}}_{p(k)}[c] = \mathbf{Y}[c] \Phi_{p(k)}^* = \sqrt{1 - \eta} \sqrt{\rho} \tau_p \mathbf{r}_k + \tilde{\mathbf{n}}_{p(k)}[c], \quad (28)$$

where $\tilde{\mathbf{n}}_{p(k)}[c] \sim \mathcal{CN}(0, \tau_p \sigma_H^2 \mathbf{I}_N)$. Next, to combat noise, the HRIS can average up the de-correlated received signals over subblocks as

$$\check{\mathbf{y}}_{p(k)} = \frac{1}{C} \sum_{c \in C} \tilde{\mathbf{y}}_{p(k)}[c] = \sqrt{1 - \eta} \sqrt{\rho} \tau_p \mathbf{r}_k + \check{\mathbf{n}}_{p(k)}, \quad (29)$$

where $\check{\mathbf{n}}_{p(k)} \sim \mathcal{CN}(0, \frac{\tau_p \sigma_H^2}{C} \mathbf{I}_N)$. The above signal can be further averaged over the antenna dimension, yielding in

$$\bar{y}_{p(k)} = \frac{1}{N} \sum_{n \in \mathcal{N}} \check{y}_{p(k),n} = \sqrt{1 - \eta} \sqrt{\rho} \tau_p \bar{r}_k + \bar{n}_{p(k)}, \quad (30)$$

where $\bar{r}_k = (1/N) \sum_{n \in \mathcal{N}} r_{k,n}$ and $\bar{n}_{p(k)} \sim \mathcal{CN}(0, \frac{\tau_p \sigma_H^2}{NC})$. After all these pre-processing steps, we are now ready to describe the probing procedure for the signal-based HRIS, which will output the detected UEs and their CSI.

Probing Procedure: Consider a pilot $t \in \mathcal{T}_p$. To detect the UEs, we use (30) and let $A_{p(k)} = \sqrt{1 - \eta} \sqrt{\rho} \tau_p \bar{r}_k$ be the complex magnitude observed if the k -th UE transmitted the t -th pilot signal, that is, $t = p(k)$. Thus, we introduce the following binary detection problem [33]:

$$\begin{aligned} \mathcal{H}_0^{(k)} : \bar{y}_{p(k)} &= \bar{n}_{p(k)}, A_{p(k)} = 0, \\ \mathcal{H}_1^{(k)} : \bar{y}_{p(k)} &= A_{p(k)} + \bar{n}_{p(k)}, A_{p(k)} \neq 0. \end{aligned} \quad (31)$$

As for the power-based case, we consider that the HRIS does not have any knowledge about the distribution of the HRIS-UE channels. Therefore, the complex magnitude A_i is assumed to be a deterministic signal unknown to the HRIS, while the noise parameter σ_H^2 is known. Based on the GLRT, the HRIS then detects a UE if [33, p. 484]

$$\mu = \frac{|\bar{y}_{p(k)}|^2}{\frac{\tau_p \sigma_H^2}{2NC}} > \epsilon_s, \quad (32)$$

with performance measured when $N \rightarrow \infty$ as

$$P_D^{(k)} = \mathcal{Q}_{\chi_4^2(\mu)}(\epsilon_s) \text{ and } P_{FA}^{(k)} = \mathcal{Q}_{\chi_4^2}(\epsilon_s), \quad (33)$$

where $P_D^{(k)}$ and $P_{FA}^{(k)}$ are the probabilities of detection and false alarm for the k -th UE, respectively. As before, the performance metrics are used to define the threshold parameter ϵ'_s . However, the measures vary with channel realizations since $A_{p(k)}$ is actually a random variable based on the channel model presented in Section III.

After performing the test in (32) over each pilot $t \in \mathcal{T}_p$, the HRIS stores the detected UEs in the set $\mathcal{K}_D = \{t | \mathcal{H}_1^{(t)} \text{ is true}, t \in \mathcal{T}_p\}$ with $\mathcal{K}_D \subseteq \mathcal{K}$. The HRIS is now ready to estimate the angle of arrival of the UEs w.r.t. each antenna. Different from the power-based case, the HRIS exploits the signal in (29) to perform such estimation. Assume again that the t -th UE transmitted the t -th pilot. Let $\mathbf{a}_k = \sqrt{1 - \eta} \sqrt{\rho} \tau_p \mathbf{r}_k$ be the complex random vector of interest, whose distribution is unknown to the HRIS; hence, the HRIS assumes that the entries of \mathbf{a}_k are deterministic values. Let $\boldsymbol{\theta}_k \in \mathbb{C}^N$ denote the angle-of-arrivals of the k -th UE $\angle \mathbf{a}_k \equiv \angle \mathbf{r}_k$. The estimation of $\boldsymbol{\theta}_k$ is based on rewriting the signal in (29) as: $\check{\mathbf{y}}_{p(k)} = \mathbf{a}_k + \check{\mathbf{n}}_{p(k)}$. Then, the HRIS estimates $\boldsymbol{\theta}_k$ as

$$\hat{\boldsymbol{\theta}}_k = \exp \left(j \arctan \left(\frac{\Im(\check{\mathbf{y}}_{p(k)})}{\Re(\check{\mathbf{y}}_{p(k)})} \right) \right), \quad (34)$$

where the exp and arctan functions are applied element-wise over the vector. The estimation error can be numerically approximated based on the fact that $\check{\mathbf{y}}_{p(k)} \sim \mathcal{CN}(\mathbf{a}_k, \frac{\tau_p \sigma_H^2}{C} \mathbf{I}_N)$. However, the estimation error varies with the channel realizations since \mathbf{a}_k is actually a random vector based on the channel model introduced in Section III. The local CSI is

$$\hat{\boldsymbol{\Theta}}_k = \text{diag}(\hat{\boldsymbol{\theta}}_k) \quad (35)$$

Again, we compute the weight ω_k to measure the importance of the k -th UE to the HRIS as

$$\omega_k = \frac{\|\check{\mathbf{y}}_{p(k)}\|_2}{\sum_{i \in \mathcal{K}_D} \|\check{\mathbf{y}}_{p(i)}\|_2}. \quad (36)$$

E. Reflection Mode

In the reflection mode, the HRIS loads a reflection configuration to support the UL data traffic and another to support the DL data traffic. Since we have assumed channel reciprocity, the reflection configuration for the UL is simply the complex conjugate of the one during DL. Therefore, we focus on the design of a single reflection configuration here. Moreover, recall that the HRIS is fully synchronized with the TDD protocol, hence it knows when to switch from UL to DL. Let $\hat{\boldsymbol{\Theta}}_R$ be the UL reflection configuration. Motivated by [7], our goal is to find $\hat{\boldsymbol{\Theta}}_R$ that maximizes the signal-to-noise ratio (SNR) of the detected UEs by using the CSI that the HRIS obtained while probing. Having this goal in mind and based on the outputs of the probe mode $\hat{\boldsymbol{\Theta}}_k$, ω_k 's as in (25), (26) and (35), (36) the reflection configuration is obtained as

$$\hat{\boldsymbol{\Theta}}_R = \boldsymbol{\Theta}_B \circ \sum_{k \in \mathcal{K}_D} \omega_k \hat{\boldsymbol{\Theta}}_k^*, \quad (37)$$

where \mathcal{K}_D is the set of detected UEs and $\boldsymbol{\Theta}_B = \text{diag}(\mathbf{a}_H(\mathbf{b}))$ denotes the CSI of the HRIS-BS channel \mathbf{G} in (6), which is assumed to be perfectly known. Note that the HRIS would like to load the following reflection configuration if the HRIS probe was perfect, meaning that all UEs were detected and their CSI perfectly estimated: $\boldsymbol{\Theta}_R = \boldsymbol{\Theta}_B \circ \sum_{k \in \mathcal{K}} \omega_k \text{diag}(\boldsymbol{\theta}_k)^*$ with $\boldsymbol{\theta}_k = \exp(j \arctan(\Im(\mathbf{r}_k)/\Re(\mathbf{r}_k)))$, and $\omega_k = \|\mathbf{r}_k\|_2 / \sum_{i \in \mathcal{K}} \|\mathbf{r}_i\|_2$. Therefore, a way to measure how good the operation of the HRIS is based on the following normalized mean-squared error (NMSE):

$$\text{NMSE}_H(C) = \frac{\|\hat{\boldsymbol{\theta}}_R - \boldsymbol{\theta}_R\|_2^2}{\|\boldsymbol{\theta}_R\|_2^2}, \quad (38)$$

where $\hat{\boldsymbol{\theta}}_R$ and $\boldsymbol{\theta}_R$ are the diagonals of $\hat{\boldsymbol{\Theta}}_R$ and $\boldsymbol{\Theta}_R$, respectively, and (C) stress that this measure depends on the choice of the probing duration τ_{prob} or, equivalently, C , while the other parameters remain fixed. Moreover, observe that $\text{NMSE}_H(C)$ also depends on the HRIS hardware architecture and statically varies with both channel and noise realizations.

V. HRIS-ASSISTED MASSIVE MIMO

In this section, we describe how the mMIMO network works when assisted by the self-configuring HRIS and by following the proposed orchestration protocol. First, we derive the mean-squared error (MSE) of the CHEST phase, showing the impact of the probe distortion as in Definition 1. Second, we present a lower bound for the spectral efficiency (SE) of a UE during the COMM phase, while taking into consideration the estimated equivalent channel and the HRIS reflection mode. For simplicity, we consider that the COMM phase is just comprised of UL traffic, that is, $\tau_d = 0$ and $\tau_u = \tau_c - L\tau_p$. The extension for the DL case is considered straightforward. Finally, we provide a way to numerically analyze the main consequences of the self-configuring trade-off (see Definition 2) over the network performance.

A. CHEST phase

According to eq. (1) and Assumptions 3 and 4, the BS receives the following pilot signal $\mathbf{Z} \in \mathbb{C}^{M \times \tau_p}$ at the l -th pilot subblock

$$\mathbf{Z}[l] = \sqrt{\rho} \begin{cases} \sum_{i \in \mathcal{K}} (\mathbf{h}_{\text{DR},i} + \sqrt{\eta} \mathbf{G} \mathbf{\Theta}_P[l] \mathbf{r}_i) \boldsymbol{\Phi}_{p(i)}^\top + \mathbf{W}[l], & \text{for } l \leq C, \\ \sum_{i \in \mathcal{K}} (\mathbf{h}_{\text{DR},i} + \sqrt{\eta} \mathbf{G} \hat{\mathbf{\Theta}}_R \mathbf{r}_i) \boldsymbol{\Phi}_{p(i)}^\top + \mathbf{W}[l], & \text{o/w,} \end{cases} \quad (39)$$

where $\mathbf{W}[l]$ is the BS receiver noise with entries i.i.d. according to $\mathcal{CN}(0, \sigma_B^2)$ with σ_B^2 being the BS noise power for $l \in \mathcal{L}$. The noise is considered to be i.i.d. over pilot subblocks. Recall that $\mathbf{\Theta}_P[l]$ represents the probe configuration used during the l -th subblock, as specified in (10), and $\hat{\mathbf{\Theta}}_R$ the reflection configuration as per (37). Based on (8) and (39), we define the following equivalent channels:

$$\mathbf{h}_{\text{P},i}[l] = \mathbf{h}_{\text{DR},i} + \sqrt{\eta} \mathbf{G} \mathbf{\Theta}_P[l] \mathbf{r}_i \quad \text{and} \quad \mathbf{h}_{\text{R},i} = \mathbf{h}_{\text{DR},i} + \sqrt{\eta} \mathbf{G} \hat{\mathbf{\Theta}}_R \mathbf{r}_i, \quad (40)$$

where $\mathbf{h}_{\text{P},i}[l]$ is the equivalent channel when the HRIS operates in the probe mode, while $\mathbf{h}_{\text{R},i}$ is the equivalent channel under the reflection mode. In principle, the BS is interested in estimating $\{\mathbf{h}_{\text{R},i}\}_{i \in \mathcal{K}}$ that represents the channel state that will also be present during the COMM phase under reflection mode. However, this estimation process suffers from the probe distortion introduced by the $\mathbf{h}_{\text{P},i}[l]$'s. Since the BS is unaware of this distortion, the BS carries out the following CHEST procedure.

CHEST Procedure: For the sake of the argument, we focus on the channel estimate of the k -th UE and assume that the k -th UE transmitted the t -th pilot for $k \in \mathcal{K}$ and $t \in \mathcal{T}_p$. Let $\mathbf{Z} = [\mathbf{Z}[1], \dots, \mathbf{Z}[L]] \in \mathbb{C}^{M \times L\tau_p}$ be the horizontally concatenated matrix of all pilot subblocks received by the BS. Denote as $\boldsymbol{\Phi}_{L_t} = [\boldsymbol{\Phi}_t; \dots; \boldsymbol{\Phi}_t] \in \mathbb{C}^{L\tau_p}$ the vector containing the t -th pilot repeated L times. To estimate the equivalent channel, the BS first takes the mean of the L received copies of the pilots, yielding in

$$\bar{\mathbf{z}}_k = \frac{1}{L} \mathbf{Z} \boldsymbol{\Phi}_{L_t}^* = \underbrace{\sqrt{\rho} \tau_p \left(\frac{1}{L} \left[\sum_{l=1}^C \mathbf{h}_{P,k}[l] + (L-C) \mathbf{h}_{R,k} \right] \right)}_{=\bar{\mathbf{h}}_k} + \frac{1}{L} \sum_{l=1}^L \mathbf{w}_t[l], \quad (41)$$

where $\mathbf{w}_t[l] \sim \mathcal{CN}(\mathbf{0}, \tau_p \sigma_B^2 \mathbf{I}_M)$ is the equivalent receiver noise and $\bar{\mathbf{h}}_k \in \mathbb{C}^M$ is the averaged equivalent channel. Below, we provide the least-squares (LS) estimate of $\bar{\mathbf{h}}_k$.⁷

Corollary 1. *The LS estimate of the channel $\bar{\mathbf{h}}_k$ based on $\bar{\mathbf{z}}_k$ is $\hat{\mathbf{h}}_k = \frac{1}{\sqrt{\rho} \tau_p} \bar{\mathbf{z}}_k \sim \mathcal{CN}(\bar{\mathbf{h}}_k, \hat{\sigma}^2 \mathbf{I}_M)$, where $\hat{\sigma}^2 = \frac{1}{L} \frac{\sigma_B^2}{\rho \tau_p}$ denotes the variance of the estimate.*

Proof. The proof follows [34, p. 225]. □

We define the NMSE of the CHEST phase for the k -th UE as

$$\text{NMSE}_{\text{CHEST},k} = \mathbb{E} \left\{ \frac{\|\hat{\mathbf{h}}_k - \mathbf{h}_{R,k}\|_2^2}{\|\mathbf{h}_{R,k}\|_2^2} \right\} = \frac{M \hat{\sigma}^2 + \|\bar{\mathbf{h}}_k - \mathbf{h}_{R,k}\|_2^2}{\|\mathbf{h}_{R,k}\|_2^2}, \quad (42)$$

where the expectation is taken with respect to noise realizations. By the definition of $\mathbf{h}_{R,k}$ in (40) and using the results of Corollary 1, the NMSE can be rewritten as:

$$\text{NMSE}_{\text{CHEST},k} = \frac{\frac{M}{L} \frac{\sigma_B^2}{\rho \tau_p} + \frac{\eta}{L^2} \left\| \mathbf{G} \left(\sum_{l=1}^C \boldsymbol{\Theta}_P[l] - C \hat{\boldsymbol{\Theta}}_R \right) \mathbf{r}_k \right\|_2^2}{\frac{\eta}{L^2} \left\| \mathbf{G} \hat{\boldsymbol{\Theta}}_R \mathbf{r}_k \right\|_2^2}, \quad (43)$$

where the first term on the numerator accounts for the *true LS estimation error* if $\mathbf{h}_{R,k}$ was to be estimated without probe distortion and the second term evaluates the *HRIS probe distortion*, following Definition 1. Observe that the $\text{NMSE}_{\text{CHEST},k}$ is a random variable with respect to UE positions, channel realizations, and the HRIS hardware and their respective probe approaches.

⁷To be consistent with the design of the HRIS, we assume that the BS knows nothing about the statistics of the equivalent channel. If this was not the case, Bayesian estimation methods could be used to further improve performance.

Remark 2 (Measuring probe distortion). *From Definition 1 and eq. (43), we note the following. First, there would be no probe distortion if there was no probing phase $C = 0$ or the probing configurations were equal to the reflection configuration $\Theta_P[l] = \hat{\Theta}_R$, $\forall l$. Second, a way to measure the probe distortion is through prob. dist. level $= \|\sum_{l=1}^C \Theta_P[l] - C\hat{\Theta}_R\|_F^2 / \|\hat{\Theta}_R\|_F^2$, which measures how different are the configurations used while the HRIS probes from the reflection configuration. This measure is independent of the channel realizations, but it depends on the HRIS hardware architecture and the design of the probe and reflection modes.*

B. COMM phase

During the COMM phase, the BS exploits the obtained CSI in Corollary 1 to help decode the messages sent by the UEs, while the HRIS in the reflection mode. Let \mathbf{v}_k denote the receive combining vector of the k -th UE. By focusing on UL and a particular sample of the τ_u samples, the BS estimates the signal sent by the k -th UE as follows [27]:

$$\hat{s}_k = \mathbf{v}_k^H \mathbf{h}_{R,k} s_k + \sum_{i \in \mathcal{K}, i \neq k} \mathbf{v}_k^H \mathbf{h}_{R,i} s_i + \mathbf{v}_k^H \mathbf{o}, \quad (44)$$

where $\mathbf{h}_{R,k}$ is defined in (40), $s_i \sim \mathcal{CN}(0, \rho)$ is the random data signal transmitted by the i -th UE, and $\mathbf{o} \sim \mathcal{CN}(\mathbf{0}, \sigma_B^2 \mathbf{I}_M)$ is the BS receiver noise for $k \in \mathcal{K}$. Thus, the instantaneous UL signal-to-interference-plus-noise ratio (SINR) of the k -th UE is given by $\text{SINR}_k^{\text{UL}} = |\mathbf{v}_k^H \mathbf{h}_{R,k} s_k|^2 / (\sum_{i \in \mathcal{K}, i \neq k} |\mathbf{v}_k^H \mathbf{h}_{R,i} s_i|^2 + |\mathbf{v}_k^H \mathbf{o}|^2)$. Hence, the instantaneous UL SE of the k -th UE can be calculated as $\text{SE}_k^{\text{UL}} = \frac{\tau_u}{\tau_c} \log_2 (1 + \text{SINR}_k) = \frac{\tau_u}{\tau_{\text{chest}} + \tau_{\text{comm}}} \log_2 (1 + \text{SINR}_k^{\text{UL}})$. We can use the use-and-then-forget (UatF) bound to estimate the above measure as follows [27].

Corollary 2. *The UL SE of the k -th UE can be lower bounded on average w.r.t. signal and noise realizations as*

$$\underline{\text{SE}}_k^{\text{UL}} = \frac{\tau_u}{\tau_c} \log_2 \left(1 + \underline{\text{SINR}}_k^{\text{UL}} \right), \text{ where } \underline{\text{SINR}}_k^{\text{UL}} = \frac{\rho \mathbb{E}\{|\mathbf{v}_k^H \mathbf{h}_{R,k}|^2\}}{\rho \sum_{i=1, i \neq k}^K \mathbb{E}\{|\mathbf{v}_k^H \mathbf{h}_{R,i}|^2\} + \mathbb{E}\{|\mathbf{v}_k^H \mathbf{o}|^2\}}. \quad (45)$$

Proof. The proof follows the same arguments from [27]. \square

C. Analysis: Self-Configuring Trade-Off

Based on Definition 2, we are now in a position to present a way to numerically evaluate how the self-configuring trade-off affects the performance of the network. From Corollary 2, we note that there are two main drawbacks from the HRIS operation. First, the numerator of the SINR is

not maximized due to probe distortion. Second, the first term of the denominator can be further increased because the reflected channels of the UEs are now spatially correlated, since all of them depend on the same reflection configuration $\hat{\mathbf{\Theta}}_R$. Therefore, a way to measure the impact of the HRIS performance is based on the lower bound of the signal-to-interference ratio (SIR)

$$\underline{\text{SIR}}_k = \frac{\mathbb{E}\{|\mathbf{v}_k^H \mathbf{h}_{R,k}|^2\}}{\sum_{i=1, i \neq k}^K \mathbb{E}\{|\mathbf{v}_k^H \mathbf{h}_{R,i}|^2\}}. \quad (46)$$

If the above metric is less than 1, the two undesirable effects mentioned above dominate, and the HRIS does not help to improve the network performance. This is a consequence of the fact that increasing inter-user interference for HRIS-assisted mMIMO systems [11], [35].

VI. NUMERICAL RESULTS

We now evaluate the performance of our orchestration framework and numerically analyze the self-configuring trade-off.⁸ Table I reports the simulation parameters employed, which are motivated by the scenario introduced in [27] with a system bandwidth of 20 MHz and the pathloss multiplicative constant set as $\gamma_0 = 1$ to better observe the effect of distance and difference in pathloss exponents. The parameters are subject to change during the numerical evaluation. The HRIS is located at the origin of our coordinate system. The BS is then placed at a distance of 1 km from the HRIS on the normal line to the origin. The UEs are randomly placed within a ring that has the RIS as the center. The inner radius of the ring is set to satisfy the far-field propagation condition from the HRIS [28], while the outer radius is set to be 100 meters. This scenario corresponds to the case in which the BS does not have good channel conditions towards the UEs since they are located in the cell edge and, consequently, a HRIS is placed to improve the quality of service. The NLoS powers σ_{DR}^2 and σ_{RR}^2 are chosen in such a way that the NLoS power is on average 10% of the LoS ones. The BS receiver noise $\sigma_H^2 = -94$ dBm comprises the thermal noise over a system bandwidth of 20 MHz and a noise figure of 7 dB in the receiver hardware. The quality of the HRIS hardware is considered to be worse than the one at the BS, having a noise figure of 10 dB [36], and resulting in $\sigma_H = -91$ dBm. Finally, to evaluate the probe distortion in its worse case, we assume that the CHEST phase takes $\tau_{\text{chest}} = 64$ samples, which is half of the coherence interval of $\tau_c = 128$ samples [27]. Therefore, we set $L = \frac{64}{\tau_p} = 16$ pilot subblocks.

⁸The code to reproduce the figures is available online on <https://github.com/victorcroisfelt/self-configuring-orchestration>.

TABLE I: Simulation Parameters

Parameter	Value	Parameter	Value
carrier frequency, f_c	28 GHz	HRIS pathloss, β_H	2
num. of BS antennas, M	64	NLoS power, $\sigma_{DR}^2, \sigma_{RR}^2$	$6.1848 \cdot 10^{-11}, 5.9603 \cdot 10^{-4}$
num. of UEs, $K_{\max} = K$	4	receive noise powers, σ_H^2, σ_B^2	-91, -94 dBm
num. of HRIS elements, N	32	UL transmit power, ρ	10 dBm
HRIS reflection coefficient η	0.99	samples per coherence block, τ_c	128
BS pathloss, β_B	3.76	num. pilots, τ_p	K

A. HRIS performance

We start by evaluating the operation of the HRIS modes by varying the following parameters: the number of probe subblocks C , the probability of false alarm P_{FA} in (23) and (33), and $1 - \eta$ that specifies how much power is absorbed by the HRIS. In principle, we are interested in very low values of η . The performance of the HRIS probe mode is evaluated by the probability of detection in (23) and (33). Fig. 6a shows the worst-case average probability of detection at the HRIS, where the worst-case represents the minimum detection probability obtained when varying $C \in \{1, 2, \dots, 16\}$. For the signal-based HRIS, one can note that the detection performance varies very little and is almost perfect, reaching 1 even with very low values of η . This happens because the noise power in (30) is reduced by a factor of $\frac{\tau_p}{NC}$ with $N \gg \tau_p$. Hence, because the signal-based HRIS can average the received signal over all of its elements, it can detect the UEs almost perfectly due also to the fact that the UEs are close to the HRIS. Meanwhile, for the power-based HRIS, one can note that the performance varies greatly with the fraction of power absorbed by the HRIS. The reason for this is that the noise power is now increased by a factor of N in (15) since the signals are superimposed in the RF-combiner shown in Fig. 5. Hence, the power-based HRIS needs a greater absorption capability to get a good detection performance.

It is worth noting that C influences the probe modes of each HRIS hardware architecture in different ways. For the power-based HRIS, C increases the number of probe directions, as per (11), and improves the detection performance due to the realization of the test in (22) over each one of these directions; after that, the final detection test is to take a logical OR operation over all these realizations. For the signal-based HRIS, C reduces the noise power in (30) since the signal can be digitally averaged out over C .

Based on Fig. 6, we select a target $P_{FA} = 10^{-3}$ and $\eta = 0.99$ to ensure a worst-case

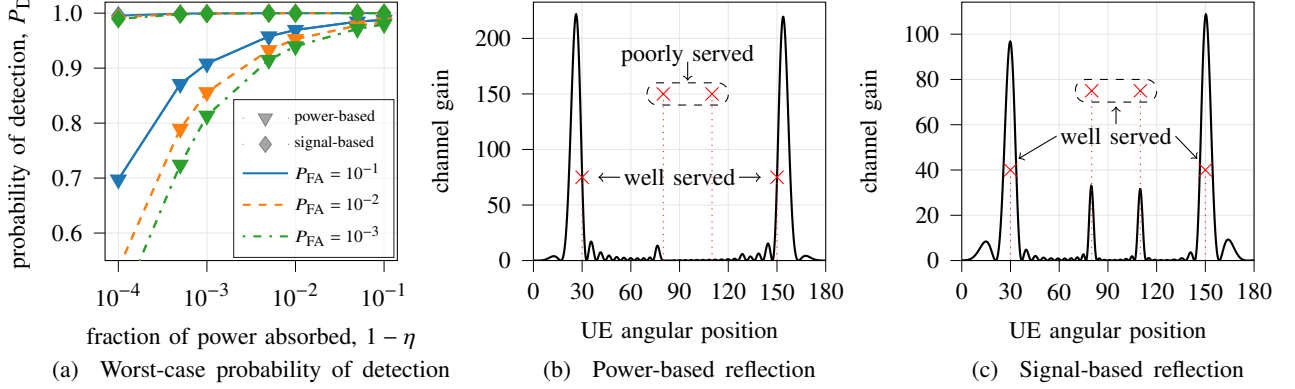


Fig. 6: HRIS probability of detection, and example of reflection configuration with power- and signal-based architecture. In Figs. 6b and 6c, ‘X’ marks represent four UEs positioned as (d_k, θ_k) : $(10, 30^\circ)$, $(20, 80^\circ)$, $(20, 110^\circ)$, and $(10, 150^\circ)$ w/ $C = 8$.

probability of detection of at least 90% for both hardware architectures. With that, the worst-case average NMSE_H in (38) evaluates to 1.97 and $1.51 \cdot 10^{-4}$ for the power- and signal-based HRIS, respectively. This shows that the power-based HRIS has inferior capability of correctly pointing towards the UEs since it depends on the level of spatial resolution available by setting the number of probe directions C in (11). We evaluate this in Figs. 6b and 6c, where one can see that, although the signal-based HRIS can have beams centered exactly at the angular position of the UEs, the power-based HRIS is not perfectly aligned and can miss some of the UEs due to its reduced angular resolution.

B. Network performance

We now evaluate how the network performance behaves in the presence of the self-configuring HRIS, giving greater focus to understanding the impact of the self-configuring trade-off. We introduce two baselines. First, we consider the mMIMO baseline where the HRIS is turned off to evaluate the gains brought by the HRIS. Second, we consider a genie baseline, where the BS knows when the HRIS probe mode ends and can avoid probe distortion. Moreover, we assume that the HRIS operates perfectly, that is, the HRIS detects and estimates the CSI of the UEs perfectly. Finally, we assume that the BS employs the zero-forcing (ZF) receive combiner as the choice of \mathbf{v}_k in (44) [27], [35].

Fig. 7 evaluates the different metrics of the network performance. First, Fig. 7a shows the average NMSE of the CHEST phase. One can note that the HRIS-related curves get worse with

the increase of C since this deteriorates the capability of the BS to observe a stable channel of interest, as stated in (41). Moreover, the effect of the probe distortion on CHEST can be measured by the vertical distance between the genie-baseline and the power- and signal-based HRIS curves. Note that the signal-based HRIS suffers more from probe distortion. One reason for this is because $\Theta[c]_P = \mathbf{I}_N$, $\forall c$ in the signal-based case, distributing the effect of the power distortion equally in all directions of the channel; while in the power-based case, some directions are more affected by the probe distortion than others.

Figs. 7b and 7c evaluate the performance of the COMM phase. We can note that the HRIS can essentially double the performance compared to the case in which it is turned off. For the signal-based HRIS, the performance goes down quickly with C for two reasons: i) the probe distortion affects more this architecture, as seen in Fig. 7a; and ii) the SIR is more affected in the signal-based RIS since the UEs are more spatially correlated, increasing the importance of the denominator. On the other hand, the power-based is less affected because it suffers less from probe distortion and has a SIR that does not decrease much as the estimation of the angle-of-arrival is less effective. The ripples observed in the power-based HRIS curves are because its angular resolution increases with C , as per (11), and its relationship with the way that the angle-of-arrival is estimated in (25).

One would expect that the genie baseline would have superior performance. However, despite a better NMSE, this is not proportionally translatable into network performance. This is because of spatial correlation and increased interference among the UEs, the genie baseline can perform worse than the power-based HRIS [11], [35].

VII. CONCLUSIONS

We proposed an orchestration framework that carefully integrates the HRIS operation modes to occur in parallel to an mMIMO network, that is, we analyze the extreme case that the HRIS operates completely anonymously without any type of control from other entities. We showed that our framework presents a trade-off that measures how practical is a self-configuring HRIS. In our experiments, we reveal that the self-configuring HRIS can essentially bring a two-fold gain in the performance of edge UEs when using our proposed framework. Our work also establishes the opportunity for further research avenues, for example, a better study of how to control interference among UEs due to the spatial correlation in the reflected path is needed.

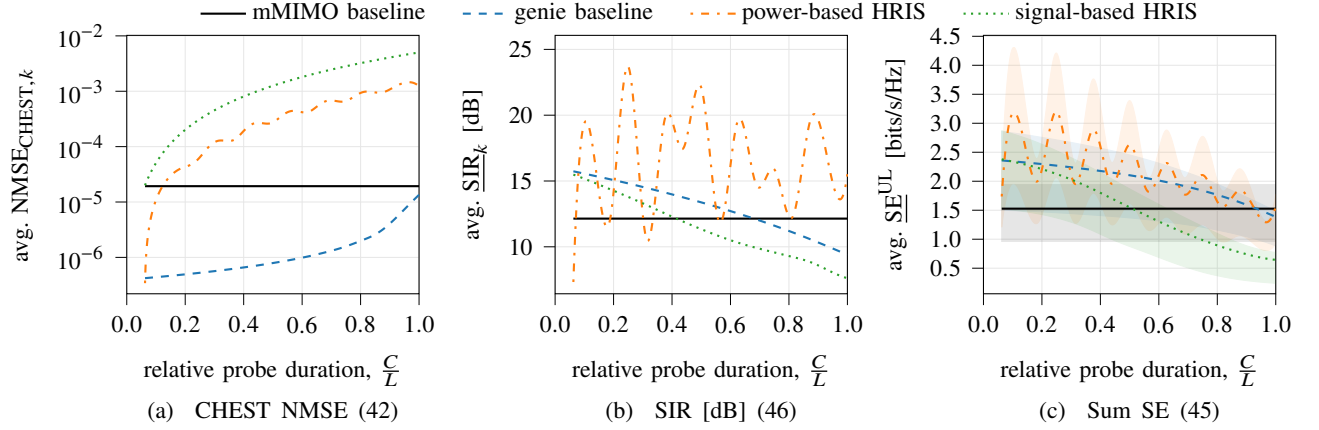


Fig. 7: Network performance as a function of the self-configuring trade-off by evaluating the ratio between the number of pilot subblocks used for probe, C , and the total number of pilot subblocks, L .

REFERENCES

- [1] M. Di Renzo *et al.*, “Smart radio environments empowered by reconfigurable intelligent surfaces: How it works, state of research, and the road ahead,” *IEEE Journal on Selected Areas in Communications*, vol. 38, no. 11, pp. 2450–2525, 2020.
- [2] C. Pan *et al.*, “Reconfigurable intelligent surfaces for 6G systems: Principles, applications, and research directions,” *IEEE Communications Magazine*, vol. 59, no. 6, pp. 14–20, 2021.
- [3] H. Yang *et al.*, “A programmable metasurface with dynamic polarization, scattering and focusing control,” *Nature, Sci Rep* 6, 35692, 2016.
- [4] E. C. Strinati *et al.*, “Wireless environment as a service enabled by reconfigurable intelligent surfaces: The RISE-6G perspective,” in *Proc. Joint European Conference on Networks and Communications 6G Summit (EuCNC/6G Summit)*, 2021, pp. 562–567.
- [5] F. Saggese *et al.*, “A framework for control channels applied to reconfigurable intelligent surfaces,” *arXiv:2303.16797 [cs.IT]*, 2023.
- [6] L. Subrt *et al.*, “Controlling the short-range propagation environment using active frequency selective surfaces,” *Radio-engineering*, vol. 19, 12 2010.
- [7] A. Albanese *et al.*, “MARISA: A self-configuring metasurfaces absorption and reflection solution towards 6G,” in *IEEE INFOCOM 2022 - IEEE Conference on Computer Communications*, 2022, pp. 250–259.
- [8] I. Alamzadeh *et al.*, “A reconfigurable intelligent surface with integrated sensing capability,” *Scientific Reports*, vol. 11, pp. 2045–2322, 2021.
- [9] E. Björnson *et al.*, “Intelligent reflecting surface versus decode-and-forward: How large surfaces are needed to beat relaying?” *IEEE Wireless Communications Letters*, vol. 9, no. 2, pp. 244–248, 2020.
- [10] —, “Massive MIMO is a reality — what is next?: Five promising research directions for antenna arrays,” *Digital Signal Processing*, vol. 94, pp. 3–20, 2019, special Issue on Source Localization in Massive MIMO.
- [11] Z. Wang *et al.*, “Intelligent reflecting surface assisted massive mimo communications,” in *2020 IEEE 21st International Workshop on Signal Processing Advances in Wireless Communications (SPAWC)*, 2020, pp. 1–5.
- [12] Y. N. Ahmed, “Large system analysis of reflecting intelligent surface aided MIMO systems with imperfect channel state information,” in *2021 28th International Conference on Telecommunications (ICT)*, 2021, pp. 1–5.

- [13] K. Zhi *et al.*, “Power scaling law analysis and phase shift optimization of RIS-aided massive MIMO systems with statistical CSI,” *IEEE Transactions on Communications*, vol. 70, no. 5, pp. 3558–3574, 2022.
- [14] —, “Is RIS-aided massive MIMO promising with ZF detectors and imperfect CSI?” *IEEE Journal on Selected Areas in Communications*, vol. 40, no. 10, pp. 3010–3026, 2022.
- [15] X. Luo *et al.*, “IRS-based TDD reciprocity breaking for pilot decontamination in massive MIMO,” *IEEE Wireless Communications Letters*, vol. 10, no. 1, pp. 102–106, 2021.
- [16] Y. Hu *et al.*, “Serving mobile users in intelligent reflecting surface assisted massive MIMO system,” *IEEE Transactions on Vehicular Technology*, vol. 71, no. 6, pp. 6384–6396, 2022.
- [17] E. Shtaiwi *et al.*, “Channel estimation approach for RIS assisted MIMO systems,” *IEEE Transactions on Cognitive Communications and Networking*, vol. 7, no. 2, pp. 452–465, 2021.
- [18] L. Wei *et al.*, “Channel estimation for RIS-empowered multi-user MISO wireless communications,” *IEEE Transactions on Communications*, vol. 69, no. 6, pp. 4144–4157, 2021.
- [19] G. Zhou *et al.*, “Channel estimation for RIS-aided multiuser millimeter-wave systems,” *IEEE Transactions on Signal Processing*, vol. 70, pp. 1478–1492, 2022.
- [20] A. M. Elbir *et al.*, “Federated learning for channel estimation in conventional and RIS-assisted massive MIMO,” *IEEE Transactions on Wireless Communications*, 2021.
- [21] G. C. Alexandropoulos *et al.*, “Hybrid reconfigurable intelligent metasurfaces: Enabling simultaneous tunable reflections and sensing for 6G wireless communications,” *arXiv preprint arXiv:2104.04690*, 2021.
- [22] N. T. Nguyen *et al.*, “Hybrid relay-reflecting intelligent surface-assisted wireless communications,” *IEEE Transactions on Vehicular Technology*, 2022.
- [23] R. Schroeder *et al.*, “Passive RIS vs. hybrid RIS: A comparative study on channel estimation,” in *2021 IEEE 93rd Vehicular Technology Conference (VTC2021-Spring)*. IEEE, 2021, pp. 1–7.
- [24] A. Taha *et al.*, “Enabling large intelligent surfaces with compressive sensing and deep learning,” *IEEE access*, vol. 9, pp. 44 304–44 321, 2021.
- [25] R. Schroeder *et al.*, “Channel estimation for hybrid RIS aided MIMO communications via atomic norm minimization,” in *2022 IEEE International Conference on Communications Workshops (ICC Workshops)*. IEEE, 2022, pp. 1219–1224.
- [26] C. Saigre-Tardif *et al.*, “A self-adaptive RIS that estimates and shapes fading rich-scattering wireless channels,” *arXiv preprint arXiv:2202.10248*, 2022.
- [27] E. Björnson *et al.*, “Massive MIMO networks: Spectral, energy, and hardware efficiency,” *Foundations and Trends® in Signal Processing*, vol. 11, no. 3-4, pp. 154–655, 2017.
- [28] V. Croisfelt *et al.*, “A random access protocol for RIS-aided wireless communications,” in *2022 IEEE 23rd International Workshop on Signal Processing Advances in Wireless Communication (SPAWC)*, 2022, pp. 1–5.
- [29] V. Croisfelt *et al.*, “Random access protocol with channel oracle enabled by a reconfigurable intelligent surface,” *arXiv:arXiv:2210.04230 [cs.IT]*, Oct. 2022.
- [30] J. Yuan *et al.*, “Channel tracking for RIS-enabled multi-user SIMO systems in time-varying wireless channels,” in *2022 IEEE International Conference on Communications Workshops (ICC Workshops)*, 2022, pp. 145–150.
- [31] L. Dai *et al.*, “Reconfigurable intelligent surface-based wireless communications: Antenna design, prototyping, and experimental results,” *IEEE Access*, vol. 8, pp. 45 913–45 923, 2020.
- [32] B. Xu *et al.*, “Reconfigurable intelligent surface configuration and deployment in three-dimensional scenarios,” in *2021 IEEE International Conference on Communications Workshops (ICC Workshops)*, 2021, pp. 1–6.
- [33] S. M. Kay, *Fundamentals of Statistical Signal Processing: Detection Theory*. Prentice Hall, 1997.
- [34] —, *Fundamentals of Statistical Signal Processing: Estimation Theory*. Prentice Hall, 1997.

- [35] Z. Wang *et al.*, “Massive MIMO communication with intelligent reflecting surface,” *IEEE Transactions on Wireless Communications*, pp. 1–1, 2022.
- [36] A. F. Molisch, *Wireless Communications*, 2nd ed. Wiley Publishing, 2011.